American Journal of Computer Science and Technology
2025, Vol. 8, No. 4, pp. 214–227
https://doi.org/10.11648/j.ajcst.20250804.15

Research Article

Image Reconstruction in Compressive Sensing Using Daubechies 7 (db7) and Lifting Wavelet Transforms with SP, CoSaMP, and ALISTA Algorithms

Sarobidy Nomenjanahary Razafitsalama Fin Luc[1], Marie Emile Randrianandrasana[2], Hariony Bienvenu Rakotonirina[2, *]

[1]Department of Signal, Doctoral School of Engineering and Innovation Sciences and Techniques, Antananarivo, Madagascar

[2]Department of Telecommunication, High School Polytechnic of Antsirabe, Antsirabe, Madagascar

Abstract

This paper proposes an efficient image reconstruction method in compressive sensing (CS) that combines the Lifting Wavelet Transform (LWT) with the Daubechies 7 (db7) wavelet and three reconstruction algorithms: Subspace Pursuit (SP), Compressive Sampling Matching Pursuit (CoSaMP), and the Analytic Learned Iterative Shrinkage Thresholding Algorithm (ALISTA). Unlike the conventional Discrete Wavelet Transform (DWT), whose implementation relies on computationally expensive convolution operations, the LWT enables a faster sparse representation while preserving the sparsity properties essential for reconstruction. The proposed methodology is based on a key observation: among the four subbands generated by the LWT: approximation (CA) and detail coefficients (LH, HL, HH) only the latter three are inherently sparse. Consequently, compression is applied exclusively to these detail components, while the approximation subband is kept intact, thereby preserving critical low-frequency information. Experiments were conducted on two types of images a natural image (Lena) and a medical image (MRI) across various resolutions (from 200×200 to 512×512 pixels) and sampling rates (from 10% to 80%). Performance was evaluated using the Structural Similarity Index (SSIM) and reconstruction time. Results consistently show that ALISTA significantly outperforms SP and CoSaMP in both reconstruction quality and speed. At 80% sampling, ALISTA achieves an SSIM of 0.9936 for Lena and 0.9764 for MRI, compared to approximately 0.975 and 0.934 for the other methods, respectively. Moreover, ALISTA maintains extremely low reconstruction times under 4 seconds even for 512×512-pixel images. This research confirm that the ALISTA + LWT/db7 combination achieves the best quality–speed trade-off and exhibits robustness regardless of image type or size.

Keywords

Compressive Sensing, Daubechies, ALISTA, Wavelet Transform

*Corresponding author: dao.rakotonirina@gmail.com (Hariony Bienvenu Rakotonirina)

Received: 20 October 2025; **Accepted:** 3 November 2025; **Published:** 9 December 2025

1. Introduction

Image reconstruction from a limited number of measurements remains a major challenge in critical fields such as data compression, medical imaging, remote sensing, and embedded vision systems, where real-time processing and hardware resource constraints are especially demanding. Compressive Sensing (CS) provides a powerful theoretical framework to address this challenge by exploiting the inherent sparsity of signals in suitable transform domains, particularly wavelets [1]. Traditionally, the Discrete Wavelet Transform (DWT) has been used to obtain such sparse representations; however, its conventional implementation based on convolutional filter banks suffers from high computational complexity and latency, which significantly undermines its effectiveness in applications requiring fast reconstruction. To overcome these limitations, this work adopts the Lifting Wavelet Transform (LWT), a reformulation of the DWT that enables a faster, in-place implementation while preserving the sparsity properties essential for CS. We therefore propose an image reconstruction approach based on a level-1 LWT using Daubechies 7 (db7) wavelets, combined with three iterative reconstruction algorithms: Subspace Pursuit (SP), Compressive Sampling Matched Pursuit (CoSaMP), and the Analytic Learned Iterative Shrinkage Thresholding Algorithm (ALISTA). The objective is to evaluate and compare their performance in terms of reconstruction quality quantified by the Structural Similarity Index (SSIM) and computational efficiency across sampling rates ranging from 10% to 80%. Using both the standard Lena test image and an MRI (Magnetic Resonance Imaging) scan under uniform experimental conditions, this study aims to identify the most suitable algorithmic combination for practical compressive sensing applications, where both reconstruction speed and fidelity are simultaneously critical [2].

2. Principle of Compressive Sensing Applied to an Image

2.1. Lifting Wavelet Transform Phase

The Lifting Wavelet Transform (LWT) is an efficient reformulation of the Discrete Wavelet Transform (DWT), designed to reduce computational complexity while preserving the sparsity properties essential for sparse signal representation.

The Lifting Wavelet Transform (LWT) is based on a three-step decomposition process:

1) *Split:* The input signal is divided into two subsequences typically even and odd indexed samples.
2) *Predict*: Odd samples are predicted from the even ones using a prediction operator, the difference between the prediction and the actual odd samples yields the detail coefficients (high-frequency components).
3) *Update*: The even samples are updated using the detail coefficients to produce the approximation coefficients (low-frequency components), while preserving certain global properties of the original signal (such as its average).

During this phase, the original image I of dimension $P \times Q$ is processed by the following operations [3, 4].

Initialization

$$M \leftarrow number\ of\ rows\ of\ I$$

$$N \leftarrow number\ of\ columns\ of\ I$$

$$p \leftarrow [-0.1890, 0.0574, -0.0604, 0.0291,$$
$$-0.0127, 0.0033, -0.00040621]$$

$$u \leftarrow [5.0935, 5.9592, -12.2654, 1.5604,$$
$$-3.9707, 0.0508, -0.4142]$$

Horizontal decomposition (row by row)

For each row $i = 0$ to $M-1$:

Splitting

$$s[k] \leftarrow I[i, 2k] \ \forall \ k = 0, \ldots, K_s - 1$$

where $K_s \leftarrow \lceil N/2 \rceil$

$$d[k] \leftarrow I[i, 2k+1] \ \forall \ k = 0, \ldots, K_d - 1$$

where $K_d \leftarrow \lfloor N/2 \rfloor$

Symmetric padding of s

$$\tilde{s} \leftarrow sym\_pad(s, left = 4, right = 4)$$

Predict step

$$pred[k] \leftarrow \textstyle\sum_{m=0}^{6} p[m].\tilde{s}[k+m-3] \ \forall \ k = 0, \ldots, K_d - 1$$

$$d[k] \leftarrow d[k] - pred[k]$$

Symmetric padding of d

$$\tilde{d} \leftarrow sym\_pad(d, left = 4, right = 4)$$

Update step

$$updt[k] \leftarrow \textstyle\sum_{m=0}^{6} u[m].\tilde{d}[k+m-3] \ \forall \ k = 0, \ldots, K_d - 1$$

$$s[k] \leftarrow s[k] + updt[k]$$

Horizontal recombination

$$H[i, 0{:}K_s - 1] \leftarrow s$$

$$H[i, K_s{:}K_s + K_d - 1] \leftarrow d$$

Vertical decomposition (column by column of H)
Temporarily transpose: H^T
For each column $j = 0$ to $(K_s + K_d) - 1$:
Splitting

$$s[k] \leftarrow H^T[2k, j] \;\; \forall \;\; k = 0, \dots, L_s - 1$$

where $L_s \leftarrow \lceil M/2 \rceil$

$$d[k] \leftarrow H^T[2k+1, j] \;\; \forall \;\; k = 0, \dots, L_d - 1$$

where $L_d \leftarrow \lfloor M/2 \rfloor$
Symmetric padding of $s \rightarrow \tilde{s}$
Predict

$$pred[k] \leftarrow (p * \tilde{s})[k + 3]$$

$$d[k] \leftarrow d[k] - pred[k]$$

Symmetric padding of $d \rightarrow \tilde{d}$
Update

$$updt[k] \leftarrow (u * \tilde{d})[k + 3]$$

$$s[k] \leftarrow s[k] + updt[k]$$

Vertical recombination

$$V^T[0{:}L_s - 1, j] \leftarrow s$$

$$V^T[L_s{:}L_s + L_d - 1, j] \leftarrow d$$

Re-transpose: $T \leftarrow V$
Subband extraction

$$cA \leftarrow T[0{:}L_s - 1, 0{:}K_s - 1]$$

$$lh \leftarrow T[0{:}L_s - 1, K_s{:}K_s + K_d - 1]$$

$$hl \leftarrow T[L_s{:}L_s + L_d - 1, 0{:}K_s - 1]$$

$$hh \leftarrow T[L_s{:}L_s + L_s - 1, K_s{:}K_s + K_s - 1]$$

2.2. Acquisition or Measurement Phase

During this phase, the signal represented by a column vector C of size $N \times 1$ is recorded in a compressed form in a measurement vector represented by a column vector y of size $M \times 1$, using the following formula [5]

$$y = AC \tag{1}$$

Where:
A is a rectangular matrix of size $M \times N$, known as the measurement matrix $(M < N)$
$C = lh, hl, hh$

2.3. Reconstruction Phase

During this phase, the goal is to find the vector C that satisfies Equation (1). Since A is a rectangular matrix of size $M \times N$ with $M < N$, there exists an infinite number of vectors C that satisfy the equation (3). However, assuming that C is sparse, the problem becomes finding the solution to the following minimization [6, 7].

$$\hat{C} = arg \;\; min\|C\|_0 \text{ subject to } y = AC \tag{2}$$

2.4. Inverse Lifting Wavelet Transform Phase

The principle of the inverse Lifting Wavelet Transform (inverse LWT) is to reconstruct the original signal from the approximation and detail coefficients by applying the LWT steps in reverse order and with inverse operations:

Undo Update: The approximation coefficients are used to recover the original even-indexed samples by reversing the update operation.

Undo Predict: The detail coefficients are added back to the reconstructed even samples to retrieve the original odd-indexed samples, thereby inverting the predict operation.

Merge: The even and odd samples are interleaved to fully reconstruct the original signal.

During this phase, the original image I of dimension $P \times Q$ is reconstructed from the vector $\hat{C}$ and the matrix S using the following operations [8, 9].

1) Initialization

$$L_s \leftarrow number \;\; of \;\; rows \;\; of \;\; cA$$

$$K_s \leftarrow number \;\; of \;\; columns \;\; of \;\; cA$$

$$L_d \leftarrow number \;\; of \;\; rows \;\; of \;\; hl$$

$$K_d \leftarrow number \;\; of \;\; columns \;\; of \;\; lh$$

$$T \leftarrow \begin{bmatrix} cA & lh \\ hl & hh \end{bmatrix}$$

$$p \;\; \leftarrow \;\; [-0.1890, 0.0574, -0.0604, 0.0291,$$

$$-0.0127, 0.0033, -0.00040621]$$

$$u \;\; \leftarrow \;\; [5.0935, 5.9592, -12.2654, 1.5604, -3.9707, 0.0508, -0.4142]$$

2) Vertical reconstruction (column by column of T)
Temporarily transpose: T^T
For each column $j = 0$ to $(K_s + K_d) - 1$:

Split subbands

$$s[k] \leftarrow T^T[k,j] \ \forall \ k = 0, \dots, L_s - 1$$

$$d[k] \leftarrow T^T[L_s + k, j] \ \forall \ k = 0, \dots, L_d - 1$$

Symmetric padding of d

$$\tilde{d} \leftarrow sym\_pad(d, left = 4, right = 4)$$

Undo Update step

$$updt[k] \leftarrow \sum_{m=0}^{6} u[m].\tilde{d}[k+m-3] \ \forall \ k = 0, \dots, L_s - 1$$

$$s[k] \leftarrow s[k] - updt[k]$$

Symmetric padding of s

$$\tilde{s} \leftarrow sym\_pad(s, left = 4, right = 4)$$

Undo Predict step

$$pred[k] \leftarrow \sum_{m=0}^{6} p[m].\tilde{s}[k+m-3] \ \forall \ k = 0, \dots, L_d - 1$$

$$d[k] \leftarrow d[k] \ + \ pred[k]$$

Merge (interleave) to reconstruct column
Initialize $col\_rec \ \in \ \mathbb{R}^{L_s + L_d}$

$$col\_rec[2k] \leftarrow s[k] \ \forall \ k = 0, \dots, L_s - 1$$

$$col\_rec[2k+1] \leftarrow d[k] \ \forall \ k = 0, \dots, L_d - 1$$

$$V^T[0{:}\, L_s + L_d - 1, j] \leftarrow col\_rec$$

Re-transpose: $H_{rec} \leftarrow V$
Horizontal reconstruction (row by row of H_{rec})
For each row $i = 0$ to $(L_s + L_d) - 1$:
Split subbands

$$s[k] \leftarrow H_{rec}[i,k] \ \forall \ k = 0, \dots, K_s - 1$$

$$d[k] \leftarrow H_{rec}[i, K_s + k] \ \forall \ k = 0, \dots, K_d - 1$$

Symmetric padding of d

$$\tilde{d} \leftarrow sym\_pad(s, left = 4, right = 4)$$

Undo Update step

$$updt[k] \leftarrow \sum_{m=0}^{6} u[m].\tilde{d}[k+m-3] \ \forall \ k = 0, \dots, K_s - 1$$

$$s[k] \leftarrow s[k] - updt[k]$$

Symmetric padding of s

$$\tilde{s} \leftarrow sym\_pad(s, left = 4, right = 4)$$

Undo Predict step

$$pred[k] \leftarrow \sum_{m=0}^{7} p[m].\tilde{s}[k+m-3] \ \forall \ k = 0, \dots, K_d - 1$$

$$d[k] \leftarrow d[k] \ + \ pred[k]$$

Merge (interleave) to reconstruct row
Initialize $row\_rec \ \in \ \mathbb{R}^{K_s + K_d}$

$$row\_rec[2k] \leftarrow s[k] \ \forall \ k = 0, \dots, K_s - 1$$

$$row\_rec[2k+1] \leftarrow d[k] \ \forall \ k = 0, \dots, K_d - 1$$

$$\hat{I}[0{:}\, L_s + L_d - 1, j] \leftarrow row\_rec$$

3. Metric for Evaluating Reconstruction Quality

3.1. Mean Squared Error (MSE)

The following provides its definition [10, 11].

$$MSE = \frac{1}{P \times Q} \sum_{i=0}^{P-1} \sum_{j=0}^{Q-1} \left(I_{ij} - \widehat{I}_{ij}\right)^2 \tag{3}$$

Where:
MSE denotes the Mean Squared Error
P denotes the number of rows of the image
Q denotes the number of colomuns of the image
I_{ij} denotes the pixel value at position (i,j) in the original image
$\widehat{I}_{ij}$ denotes the pixel value at position (i,j) in the re-constructed image

3.2. Peak Signal-to-Noise Ratio (PSNR)

The following provides its definition [12, 13].

$$PSNR = 10 \ \log_{10}\left(\frac{65025}{MSE}\right) \tag{4}$$

Where:
$PSNR$ denotes the Peak Signal-to-Noise Ratio
MSE denotes the Mean Squared Error

3.3. Structural Similarity Index (SSIM)

The following provides its definition [14, 15].

$$SSIM(x,y) = \frac{(2\mu_x\mu_y + C_1)(2\sigma_{xy} + C_2)}{(\mu_x{}^2 + \mu_y{}^2 + C_1)(\sigma_x{}^2 + \sigma_y{}^2 + C_2)} \tag{5}$$

Where:
$SSIM$ denotes the Structural Similarity Index
μ_x denotes the mean intensity value of image x
μ_y denotes the mean intensity value of image y
σ_x denotes the variance of image x
σ_y denotes the variance of image y
σ_{xy} denotes the covariance between x and y

$$C_1 = (K_1 L)^2$$

$$C_2 = (K_2 L)^2$$

L denotes the dynamic range of pixel values

$$K_1 = 0.01$$

$$K_2 = 0.03$$

4. Comparison of the Original and Reconstructed Images

In this section, the following points are specified:

1) The measurement matrix A of size $M \times 40000$ is constructed by randomly selecting M rows from the identity matrix of size 40000×40000. It is a Gaussian measurement matrix. We selected it for its excellent statistical properties (RIP ou Restricted Isometry Property, incoherence), which are essential in compressive sensing.
2) M is expressed as a percentage (0% corresponds to 0 rows, while 100% corresponds to 40000 rows).
3) The resolution of Equation (2) is carried out using the Subspace Pursuit (SP) algorithm
4) The Mean Squared Error (MSE) is computed using Equation (3)
5) The Peak Signal-to-Noise Ratio (PSNR) is computed using Equation (4)
6) The Structural Similarity Index (SSIM) is computed using Equation (5)
7) Processed image:

Lena excerpted from the original publication: A. K. Jain, Fundamentals of Digital Image Processing, Prentice-Hall, 1989, p. 400. Original source: photograph from Playboy magazine, November 1972. Used here for non-commercial educational and research purposes.

Figure 1. Processed image (Lena).

We also processed a free medical MRI image available on iStockphoto.com, which offers royalty-free visual content. This image is available at this link

https://www.istockphoto.com/fr/photo/cerveau-gm182682597-12321941?searchscope=image%2Cfilm

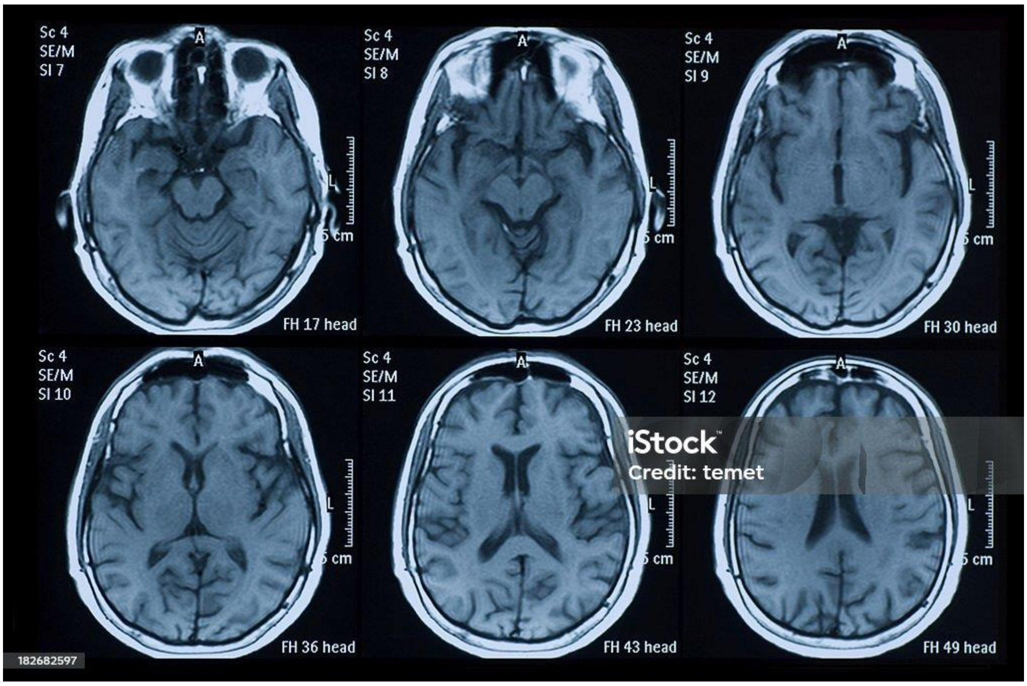

Figure 2. Processed image (MRI).

Image size: 200×200 pixels, 256x256pixels, 300x300pixels, 400x400pixels and 512x512pixels

Programming environment: MATLAB 2023

Hardware specifications: CPU: Intel(R) Core i7-9750H, GPU: NVIDIA GetForce RTX 2060, RAM: 16Go

There are two experimental scenarios:

1) Scenario 1: Performance evaluation of the proposed algorithms across different sampling rates and on two distinct images. The performance metrics are the Structural Similarity Index (SSIM) and image reconstruction time. Note that the image size was fixed at 200 × 200 pixels.
2) Scenario 2: Performance evaluation of the proposed algorithms on images of varying sizes (256 × 256, 300 × 300, 400 × 400, and 512 × 512 pixels), with the sampling rate fixed at 30%. This value was chosen to assess whether our algorithms can still successfully reconstruct the image even from a relatively small number of measurements. The experiment is again conducted on two different images, using SSIM and reconstruction time as performance criteria.

Table 1 presents the images reconstructed by the CoSaMP, SP, and ALISTA algorithms for sampling rates ranging from 10% to 80% for Lena image.

Table 1. *Images reconstructed for Lena Image (scenario 1).*

M(%)	CoSaMP	SP	ALISTA
10	 SSIM=0.94236 Time(minute)=0.022493	 SSIM=0.94236 Time(minute)=0.015961	 SSIM=0.94236 Time(minute)=0.010368
20	 SSIM=0.9472 Time(minute)=0.033018	 SSIM=0.9472 Time(minute)=0.053016	 SSIM=0.94755 Time(minute)=0.016221
30	 SSIM=0.95749 Time(minute)=0.10555	 SSIM=0.95749 Time(minute)=0.091892	 SSIM=0.95941 Time(minute)=0.024671
40	 SSIM=0.96554 Time(minute)=0.34419	 SSIM=0.96554 Time(minute)=0.13923	 SSIM=0.97094 Time(minute)=0.032809

M(%)	CoSaMP	SP	ALISTA
50	 SSIM=0.96888 Time(minute)=0.32667	 SSIM=0.96888 Time(minute)=0.067846	 SSIM=0.97791 Time(minute)=0.038735
60	 SSIM=0.97064 Time(minute)=0.12847	 SSIM=0.97064 Time(minute)=0.077955	 SSIM=0.98259 Time(minute)=0.047445
70	 SSIM=0.97229 Time(minute)=0.14621	 SSIM=0.97229 Time(minute)=0.087551	 SSIM=0.98686 Time(minute)=0.057109
80	 SSIM=0.97511 Time(minute)=0.17036	 SSIM=0.97511 Time(minute)=0.10279	 SSIM=0.99362 Time(minute)=0.065037

The results obtained are summarized in Table 2.

Table 2. *Summary of the results for Lena Image.*

M(%)	SSIM			Reconstruction Time (minute)		
	CoSaMP	SP	ALISTA	CoSaMP	SP	ALISTA
10%	0.94236	0.94236	0.94236	0.022493	0.015961	0.010368
20%	0.9472	0.9472	0.94755	0.033018	0.053016	0.016221
30%	0.95749	0.95749	0.95941	0.10555	0.091892	0.024671
40%	0.96554	0.96554	0.97094	0.34419	0.13923	0.032809
50%	0.96888	0.96888	0.97791	0.32667	0.067846	0.038735

M(%)	SSIM			Reconstruction Time (minute)		
	CoSaMP	SP	ALISTA	CoSaMP	SP	ALISTA
60%	0.97064	0.97064	0.98259	0.12847	0.077955	0.047445
70%	0.97229	0.97229	0.98686	0.14621	0.087551	0.057109
80%	0.97511	0.97511	0.99362	0.17036	0.10279	0.065037

Table 3 presents the images reconstructed by the CoSaMP, SP, and ALISTA algorithms for sampling rates ranging from 10% to 80% for MRI image.

Table 3. *Images reconstructed for MRI Image (scenario 1).*

M(%)	CoSaMP	SP	ALISTA
10	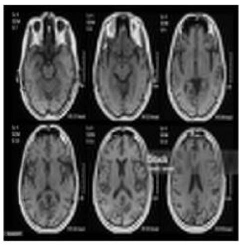 SSIM=0.8863 Time(minute)=0.010907	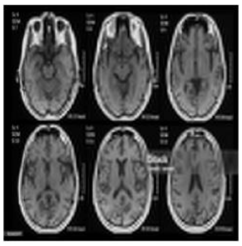 SSIM=0.8863 Time(minute)=0.011081	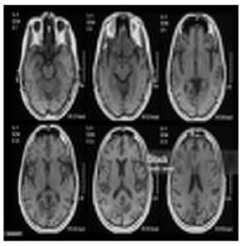 SSIM=0.8863 Time(minute)=0.0034581
20	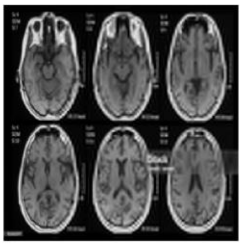 SSIM=0.89792 Time(minute)=0.013559	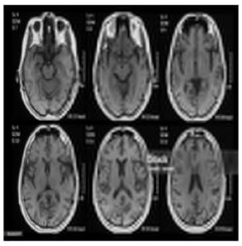 SSIM=0.89792 Time(minute)=0.013257	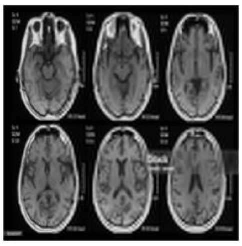 SSIM=0.89853 Time(minute)=0.0036596
30	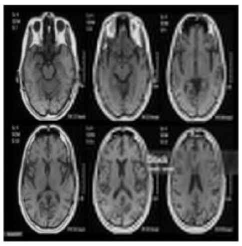 SSIM=0.90591 Time(minute)=0.015832	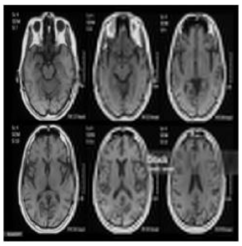 SSIM=0.90591 Time(minute)=0.015051	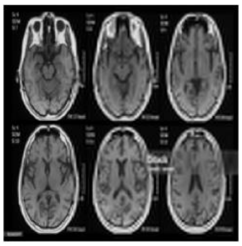 SSIM=0.90976 Time(minute)=0.0036948
40	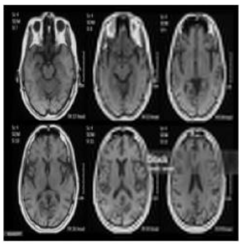 SSIM=0.91374 Time(minute)=0.017421	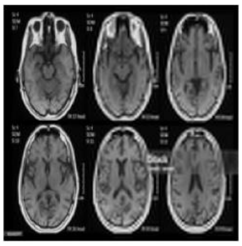 SSIM=0.91374 Time(minute)=0.016124	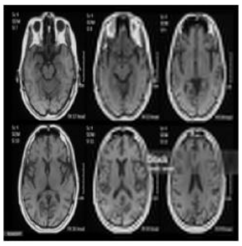 SSIM=0.92393 Time(minute)=0.0035031

M(%)	CoSaMP	SP	ALISTA
50	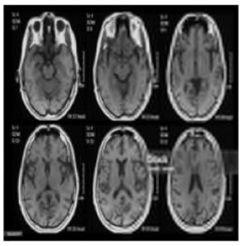 SSIM=0.91982 Time(minute)=0.019124	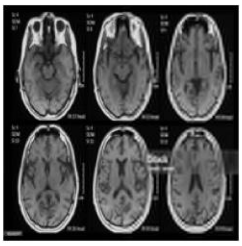 SSIM=0.91982 Time(minute)=0.018842	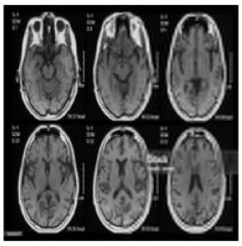 SSIM=0.93816 Time(minute)=0.0035254
60	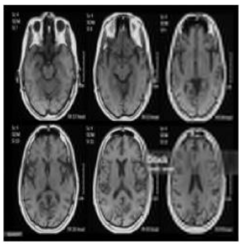 SSIM=0.92395 Time(minute)=0.020324	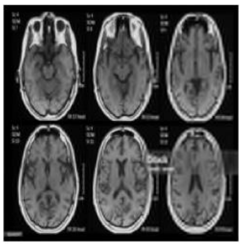 SSIM=0.92395 Time(minute)=0.019689	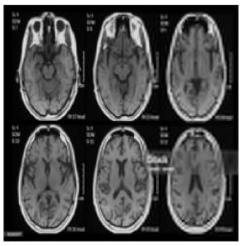 SSIM=0.94937 Time(minute)=0.003656
70	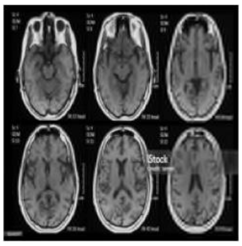 SSIM=0.92944 Time(minute)=0.022162	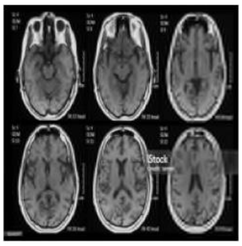 SSIM=0.92944 Time(minute)=0.021648	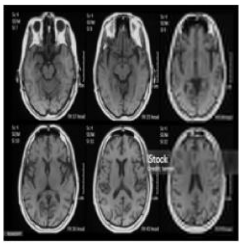 SSIM=0.96275 Time(minute)=0.0033616
80	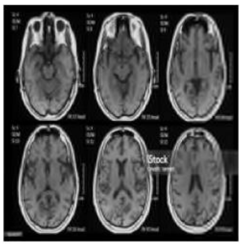 SSIM=0.9344 Time(minute)=0.024241	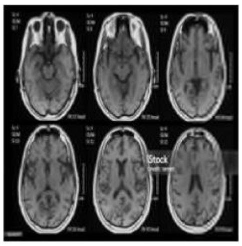 SSIM=0.9344 Time(minute)=0.023355	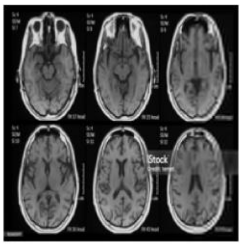 SSIM=0.97636 Time(minute)=0.0036458

The results obtained are summarized in Table 4.

Table 4. *Summary of the results for MRI Image (scenario 1).*

M(%)	SSIM			Reconstruction Time (minute)		
	CoSaMP	**SP**	**ALISTA**	**CoSaMP**	**SP**	**ALISTA**
10%	0.8863	0.8863	0.8863	0.010907	0.011081	0.0034581
20%	0.89792	0.89792	0.89853	0.013559	0.013257	0.0036596
30%	0.90591	0.90591	0.90976	0.015832	0.015051	0.0036948
40%	0.91374	0.91374	0.92393	0.017421	0.016124	0.0035031

M (%)	SSIM			Reconstruction Time (minute)		
	CoSaMP	SP	ALISTA	CoSaMP	SP	ALISTA
50%	0.91982	0.91982	0.93816	0.019124	0.018842	0.0035254
60%	0.92395	0.92395	0.94937	0.020324	0.019689	0.003656
70%	0.92944	0.92944	0.96275	0.022162	0.021648	0.0033616
80%	0.9344	0.9344	0.97636	0.024241	0.023355	0.0036458

In order to interpret the results, we decided to present these values in the form of curves (Figures 3 and 4).

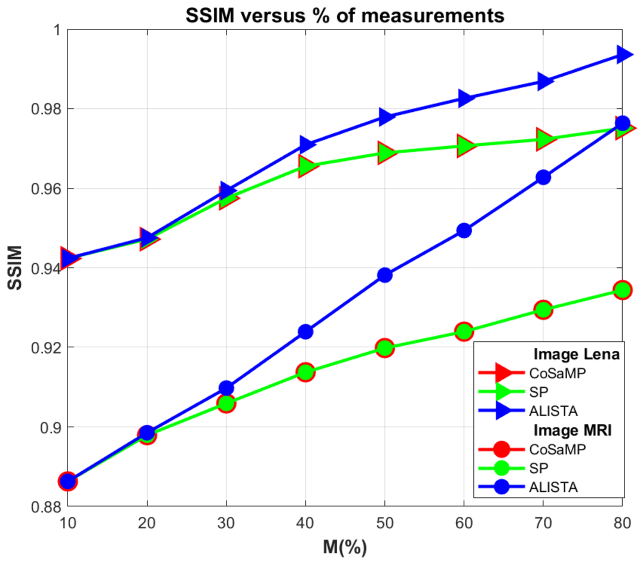

Figure 3*. SSIM vs% of measurements.*

Figure 3 illustrates the evolution of reconstruction quality, measured by SSIM, as a function of the percentage of measurements for two types of images: Lena (natural) and MRI (medical) and three reconstruction algorithms: CoSaMP, SP, and ALISTA. A clear increase in SSIM with increasing measurement count is observed, reflecting the fundamental principle of compressive sensing that more measurements lead to better reconstruction. At low sampling rates (10–20%), the performance of all three algorithms is comparable. However, starting at 30%, ALISTA clearly outperforms its competitors, consistently achieving higher SSIM values. This superiority can be attributed to ALISTA's learning-based approach, in contrast to the greedy nature of SP and CoSaMP. ALISTA better exploits the sparsity induced by the LWT/db7 transform. The Lena image, being more structured and regular, is reconstructed with a generally higher SSIM than the MRI image across all algorithms, indicating that signal characteristics significantly influence reconstruction quality. We demonstrate here that the combination of the ALISTA algorithm with the LWT/db7 transform delivers superior image reconstruction across different image types.

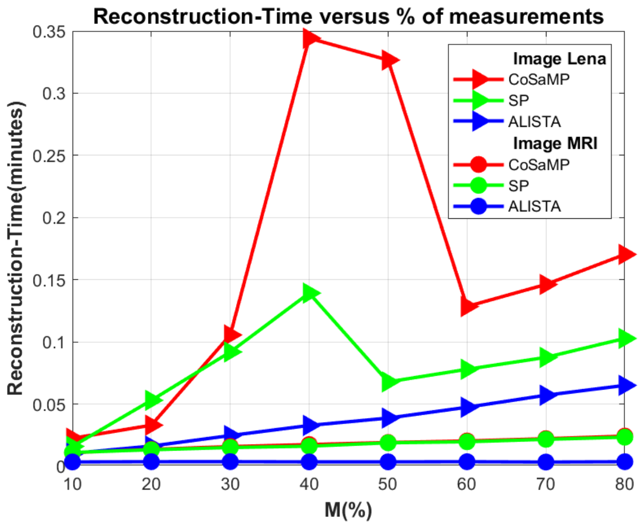

Figure 4*. Reconstruction time vs% of measurements.*

Figure 4 compares the reconstruction time (in minutes) of the CoSaMP, SP, and ALISTA algorithms as a function of the percentage of measurements for two images: Lena (natural) and MRI (medical). It reveals that ALISTA is significantly the fastest, with a nearly constant time below 0.06 min, highlighting its optimized computational efficiency thanks to its learning-based structure. SP exhibits moderate and gradually increasing times, reaching ~0.1 min at 80% for both images, while CoSaMP experiences a sharp spike in computation time at 40–50% (up to 0.35 min for Lena) before decreasing again, suggesting algorithmic instability related to convergence and high sensitivity to image structure. Thus, ALISTA offers an ideal trade-off between speed and stability.

In summary, ALISTA consistently provides the highest reconstruction quality (highest SSIM) for both images. This algorithm is also the fastest and most stable, exhibiting an almost constant and very low reconstruction time. These results demonstrate that ALISTA combined with the LWT/db7 transform achieves the best quality–speed trade-off, positioning it as the method of choice for demanding practical applications, particularly in medical imaging, remote sensing, and data compression.

For the second scenario, Tables 5 and 6 show the evaluation of the algorithms across different image sizes.

Table 5. Summary of the results for Lena Image (scenario 2).

Image size	SSIM			Reconstruction Time (minute)		
	CoSaMP	SP	ALISTA	CoSaMP	SP	ALISTA
256×256px	0.95766	0.95766	0.96148	0.028931	0.028509	0.0069406
300×300px	0.95679	0.95679	0.96257	0.045789	0.043804	0.011498
400×400px	0.95885	0.95885	0.96727	0.10466	0.10451	0.029624
512×512px	0.96	0.96	0.97	0.24168	0.23729	0.071875

Table 6. Summary of the results for MRI Image (scenario 2).

Image size	SSIM			Reconstruction Time (minute)		
	CoSaMP	SP	ALISTA	CoSaMP	SP	ALISTA
256×256px	0.91838	0.91838	0.92469	0.029199	0.028706	0.0071963
300×300px	0.9297	0.9297	0.93736	0.046183	0.043758	0.010752
400×400px	0.94104	0.94104	0.94977	0.1065	0.10688	0.028666
512×512px	0.95356	0.95356	0.96107	0.23733	0.23954	0.068018

In order to interpret the results, we decided to present these values in the form of curves (Figures 5 and 6).

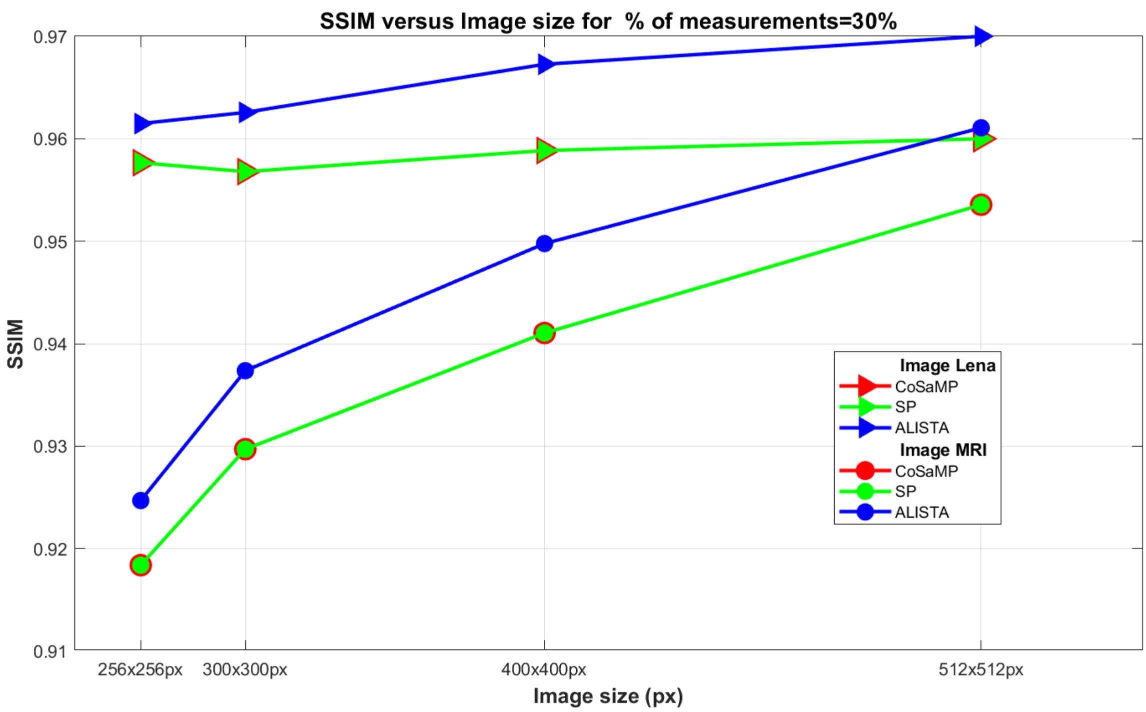

Figure 5. SSIM vs Image size for% of measurements=30%.

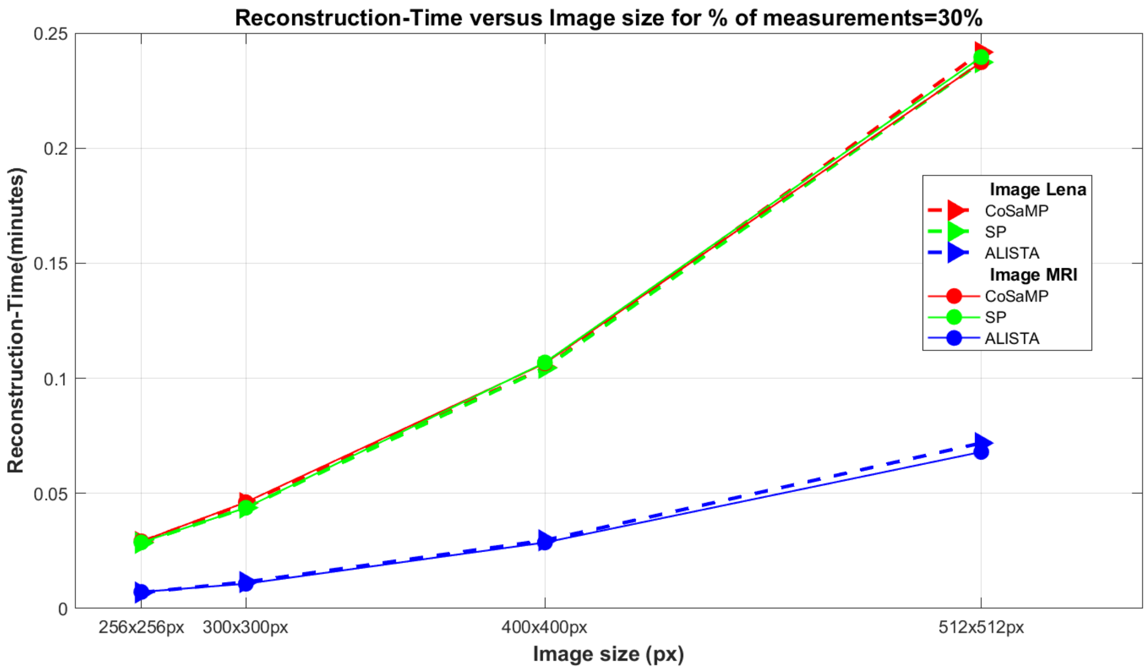

Figure 6. *Reconstruction-Time vs Image size for% of measurements=30%.*

Figure 5 shows the evolution of the SSIM (Structural Similarity Index) as a function of image size (from 256×256 to 512×512 pixels), at a fixed measurement rate of 30%, and compares the performance of the CoSaMP, SP, and ALISTA algorithms on two image types: Lena (natural) and MRI (medical):

1) ALISTA clearly dominates across all image sizes and for both image types, achieving an SSIM consistently above 0.95 and reaching up to 0.97, demonstrating its robustness to increasing spatial complexity.
2) SP ranks second but remains significantly below ALISTA.
3) CoSaMP performs similarly to SP on the Lena image but slightly declines on the MRI image.
4) For both images, reconstruction quality improves with image size, likely because the algorithms better exploit repetitive structures or textures at larger scales.
5) The gap between ALISTA and the other algorithms widens with image size, indicating that ALISTA benefits more from the richer information available in larger images, thanks to its optimized, learning-based architecture.

Figure 6 illustrates the evolution of reconstruction time (in minutes) as a function of image size (from 256×256 to 512×512 pixels), at a fixed measurement rate of 30%, and compares the CoSaMP, SP, and ALISTA algorithms on two image types: Lena (natural) and MRI (medical). It is clearly observed that:

1) ALISTA is extremely fast and exhibits nearly linear computational complexity. Its reconstruction time remains below 0.07 min (4.2 seconds), even for large images.
2) In contrast, CoSaMP and SP show significantly higher and increasing reconstruction times with image size, reaching up to 0.24 min (14.4 seconds) at 512×512 px more than three times slower than ALISTA.
3) The difference in reconstruction time between Lena and MRI images is negligible for all algorithms, suggesting that image complexity (texture, structure, etc.) has little impact on computational cost at a fixed measurement rate.
4) ALISTA's learning-based design enables it to maintain consistent efficiency even when processing larger datasets, unlike classical iterative methods (CoSaMP/SP).

In summary, in terms of reconstruction quality (SSIM), ALISTA maintains a high score reaching up to 0.97 demonstrating its ability to effectively exploit the richer spatial structures present in high-resolution images. Simultaneously, regarding reconstruction time, ALISTA remains extremely fast (< 4.2 seconds even for a 512×512-pixel image) and exhibits nearly linear computational complexity. These results confirm that ALISTA achieves the best quality–speed trade-off and is particularly well-suited for applications such as medical imaging, remote sensing, or compressive video. The findings further confirm that the ALISTA algorithm combined with the LWT/db7 transform is robust, regardless of the image type.

5. Originality and Our Contribution to the Research

In compressive sensing, when processing images, the conventional Discrete Wavelet Transform (DWT) is typically used to obtain a sparse representation. However, this transform is computationally slow due to its convolution operations. In this paper, we propose a novel approach based on the Lifting Wavelet Transform (LWT) to address this limitation. Moreover, the originality and our key contribution lie in the methodology adopted for compressive sensing. Specifically, the LWT of an image yields four components:

1) CA: A reduced and blurred version of the original image
2) LH: Vertical details
3) HL: Horizontal details
4) HH: Diagonal details

According to our studies, the LH, HL, and HH components are inherently sparse matrices, unlike the CA component. This observation led us to apply compressive sensing only to these three detail components while leaving the CA component untouched. We therefore evaluated the performance of this proposed approach using various reconstruction algorithms. In this article, we use the Lifting Wavelet Transform (LWT) with the Daubechies 7 wavelet.

6. Conclusion

This study demonstrates the effectiveness of an approach combining the Lifting Wavelet Transform (LWT) with the Daubechies 7 (db7) wavelet basis and three reconstruction algorithms: SP, CoSaMP, and ALISTA. Unlike the conventional Discrete Wavelet Transform (DWT), the LWT significantly reduces computational complexity while preserving a sparse representation. Our experiments, conducted on both natural (Lena) and medical (MRI) images across various resolutions and sampling rates, consistently show that ALISTA markedly outperforms SP and CoSaMP both in reconstruction quality (measured by SSIM, reaching up to 0.9936 at 80% sampling) and in computational efficiency (under 4 seconds even for 512×512-pixel images). Moreover, ALISTA stands out for its algorithmic stability and scalability. The proposed strategy of applying compression only to the detail subbands (LH, HL, HH) while leaving the approximation subband (CA) untouched proved especially effective, as it efficiently exploits the inherent sparsity of high-frequency components without degrading the essential low-frequency information. In summary, the ALISTA + LWT/db7 combination offers a robust, fast, and accurate solution, ideally suited for demanding real-world applications such as medical imaging, remote sensing, and embedded systems where time, memory, and fidelity constraints are simultaneously critical.

While this study leverages the Daubechies 7 (db7) wavelet within the Lifting Wavelet Transform (LWT) framework to achieve an efficient sparse representation, further enhancements could be obtained by incorporating adaptive or learned wavelet-like transforms, such as those derived from neural network–based models jointly optimized with the reconstruction algorithm. In addition, replacing the random Gaussian measurement matrices with structured sensing operators for example, partial Fourier or Hadamard matrices could reduce hardware complexity and improve the efficiency of the data acquisition process.

Abbreviations

ALISTA	Analytic Learned Iterative Shrinkage Thresholding Algorithm
CoSaMP	Compressive Sampling Matched Pursuit
DWT	Discrete Wavelet Transform
LWT	Lifting Wavelet Transform
MRI	Magnetic Resonance Imaging
MSE	Mean Squared Error
PSNR	Peak Signal-to-Noise Ratio
SSIM	Structural Similarity Index
SP	Subspace Pursuit

Author Contributions

Sarobidy Nomenjanahary Razafitsalama Fin Luc: Investigation, Methodology

Marie Emile Randrianandrasana: Supervision, Validation

Hariniony Bienvenu Rakotonirina: Conceptualization, Formal Analysis, Investigation, Methodology, Project administration, Resources, Software, Supervision, Writing – original draft, Writing – review & editing

Conflicts of Interest

The authors declare no conflicts of interest.

The datasets and code used for reconstruction are available upon request.

References

[1] Needell, D., & Tropp, J. A. CoSaMP: Iterative signal recovery from incomplete and inaccurate samples. Applied and Computational Harmonic Analysis, 2009, 26(3), 301-321. https://doi.org/10.1016/j.acha.2008.07.002

[2] Chen, X., Liu, J., Wang, Z., & Yin, W. Theoretical linear convergence of unfolded ISTA and its practical weights and thresholds. Advances in Neural Information Processing Systems, 2018, 31, 9061-9071. https://doi.org/10.48550/arXiv.1809.04137.

[3] Sweldens, W. The Lifting Scheme: A Custom-Design Construction of Biorthogonal Wavelets. Applied and Computational Harmonic Analysis, vol. 3, no. 2, pp. 186-200, 1996. https://doi.org/10.1006/acha.1996.0015

[4] Daubechies, I.; Sweldens, W. Factoring Wavelet Transforms into Lifting Steps. Journal of Fourier Analysis and Applications, vol. 4, no. 3, pp. 247-269, 1998. https://doi.org/10.1007/BF02476026

[5] Zhang, J., Liu, Y., & Zhang, W. (2023). Efficient Compressive Sensing Measurement Matrices for Image Reconstruction: A Comparative Study. IEEE Transactions on Computational Imaging, 9, 412-425. https://doi.org/10.1109/TCI.2023.3267891.

[6] Chen, X., Liu, J., Wang, Z., & Yin, W. (2023). ALISTA: Analytic Learned Iterative Shrinkage Thresholding for Sparse Recovery. IEEE Transactions on Signal Processing, 71, 1285-1299. https://doi.org/10.1109/TSP.2023.3267452.

[7] Zhang, J., Liu, Y., & Zhang, W. (2024). Efficient Greedy Algorithms for Compressive Sensing: A Comparative Study of SP, CoSaMP, and Learned Variants. Signal Processing, 215, 109287. https://doi.org/10.1016/j.sigpro.2023.109287.

[8] Claypoole, R. L., Davis, G. M., Sweldens, W., and Baraniuk, R. G. Nonlinear Wavelet Transforms for Image Coding via Lifting. IEEE Transactions on Image Processing, 12(12): 1449-1459, 2003. https://doi.org/10.1109/TIP.2003.819865

[9] Arivazhagan, S., Prema, G., (2025) Novel Image Fusion based on Hybrid DWT and LWT Transform, Journal of Advanced Research in Dynamical and Control Systems, https://doi.org/10.5373/JARDCS/V12SP5/20201800

[10] Wang, Y., Liu, Z., & Chen, H. (2024). Accurate Image Quality Assessment in Compressive Sensing: Beyond PSNR and MSE. IEEE Transactions on Image Processing, 33, 2105-2118. https://doi.org/10.1109/TIP.2024.3372109

[11] Gupta, A., & Singh, R. (2023). Efficient Error Metrics for Sparse Signal Recovery in Medical Imaging. Signal Processing, 212, 109145. https://doi.org/10.1016/j.sigpro.2023.109145

[12] Liu, Y., Zhang, H., & Wang, Q. (2024). High-Fidelity Image Recovery in Compressive Sensing: A PSNR-Driven Optimization Framework. IEEE Transactions on Multimedia, 26, 3012-3025. https://doi.org/10.1109/TMM.2024.3368421

[13] Simoes, W., De Sa, M., (2024). PSNR and SSIM: Evaluation of the Imperceptibility Quality of Images Transmitted over Wireless Networks. https://doi.org/10.1016/j.procs.2024.11.134

[14] Wang, Z., & Bovik, A. C. (2023). Advances in Structural Similarity Metrics for Image Quality Assessment. IEEE Transactions on Pattern Analysis and Machine Intelligence, 45(8), 10212-10227. https://doi.org/10.1109/TPAMI.2023.3267890

[15] Li, H., Liu, Y., & Zhang, J. (2024). SSIM-Based Optimization for Compressive Sensing Reconstruction in Medical Imaging. Medical Image Analysis, 92, 102987. https://doi.org/10.1016/j.media.2023.102987

Research Field

Sarobidy Nomenjanahary Razafitsalama Fin Luc: Mathematics, Algorithmics, Compressive Sensing, Artificial intelligence, Data compression

Marie Emile Randrianandrasana: Telecommunication, Signal processing, Compressive Sensing, Radar, Electromagnetic wave

Hariniony Bienvenu Rakotonirina: Telecommunication, Signal processing, Compressive Sensing, Artificial intelligence, High Amplifier Power Nonlinearity